Advanced Drug Delivery Reviews 72 (2014) 15–27

Contents lists available at ScienceDirect

Advanced Drug Delivery Reviews

journal homepage: www.elsevier.com/locate/addr

Recent advances in molecular, multimodal and theranostic ultrasound imaging☆

Fabian Kiessling [a,*], Stanley Fokong [a], Jessica Bzyl [a], Wiltrud Lederle [a], Moritz Palmowski [a], Twan Lammers [a,b]

[a] Department of Experimental Molecular Imaging, Helmholtz Institute for Biomedical Engineering, RWTH-Aachen University, Aachen, Germany
[b] Department of Controlled Dug Delivery, MIRA Institute for Biomedical Engineering and Technical Medicine, University of Twente, Enschede, The Netherlands

ARTICLE INFO

Available online 4 December 2013

Keywords:
Molecular imaging
Sonography
Angiogenesis
Drug delivery
Cavitation
Tumor
Cardiovascular
Blood–brain barrier
Theranostics
Nanomedicine

ABSTRACT

Ultrasound (US) imaging is an exquisite tool for the non-invasive and real-time diagnosis of many different diseases. In this context, US contrast agents can improve lesion delineation, characterization and therapy response evaluation. US contrast agents are usually micrometer-sized gas bubbles, stabilized with soft or hard shells. By conjugating antibodies to the microbubble (MB) surface, and by incorporating diagnostic agents, drugs or nucleic acids into or onto the MB shell, molecular, multimodal and theranostic MBs can be generated. We here summarize recent advances in molecular, multimodal and theranostic US imaging, and introduce concepts how such advanced MB can be generated, applied and imaged. Examples are given for their use to image and treat oncological, cardiovascular and neurological diseases. Furthermore, we discuss for which therapeutic entities incorporation into (or conjugation to) MB is meaningful, and how US-mediated MB destruction can increase their extravasation, penetration, internalization and efficacy.

Contents

☆ This review is part of the *Advanced Drug Delivery Reviews* theme issue on "Ultrasound triggered drug delivery".

* Corresponding author at: Department of Experimental Molecular Imaging, RWTH-University Aachen, Pauwelsstrasse 20, 52074 Aachen, Germany.
E-mail address: fkiessling@ukaachen.de (F. Kiessling).

0169-409X/$ – see front matter © 2013 Elsevier B.V. All rights reserved.
http://dx.doi.org/10.1016/j.addr.2013.11.013

1. Introduction

1.1. Current indications for using ultrasound imaging

Due to its non-invasive nature, low cost, broad diagnostic applicability and easy handling, ultrasound (US) imaging is the second-most used imaging modality in clinical practice after conventional x-ray radiography [1]. It is used by medical doctors from various different disciplines, including radiologists, gynecologists, cardiologists, gastroenterologists, surgeons and many more as an initial screening tool, as well as for fast-look follow-up examinations. Its ability to visualize blood flow, blood velocity and blood vessels by Power and Color Doppler further recommends US imaging for vascular diagnosis, e.g. for measuring the degree of stenosis in carotid arteries [2], and for looking at the perfusion of tumors [3] and organs after transplantation [4].

Besides these diagnostic applications, High-Intensity Focused US (HIFU) has been attracting ever more attention as a valuable therapeutic option to destroy ureteric stones [5], and to ablate benign uterus myomas and other benign and malignant tumors [6]. In this context, the acoustic energy focused to one defined spot is moved over the pathological tissue. Due to absorption of the acoustic energy and the resulting local temperature increase, the pathological tissue is destroyed. Recently, the first commercial HIFU-systems that can be used inside clinical MR scanners have been introduced which enable highly personalized and well-controlled tissue ablation by getting anatomical information about the pathology and the local temperature rise from MR imaging.

However, the diagnostic and therapeutic potential of US imaging has not yet been fully explored and translated to clinic. In this regard, US contrast agents, which are gas-filled microbubbles (MBs) stabilized by a shell made of lipids, proteins or polymers can enormously improve US imaging. In particular, the use of MB significantly expands the diagnostic potential of US for characterizing pathologies based on functional and molecular vascular characteristics. Furthermore, the use of MB-based contrast agents in US imaging offers possibilities for image-guided (theranostic) interventions. In the present manuscript, recent developments in this emerging and interdisciplinary field are summarized and discussed.

1.2. Impact of contrast-enhanced US imaging on routine clinical practice

US contrast agents in combination with contrast agent-specific US imaging techniques are increasingly accepted in routine clinical practice for diagnostic imaging of several organs and pathologies. Particular interest is given to examinations of the liver, because of the significant improvement over conventional US in both, the detection and characterization of focal liver lesions. Recent studies even show that the diagnostic performance of contrast-enhanced ultrasound (CEUS) can reach that of contrast-enhanced computed tomography (CT) and magnetic resonance imaging (MRI) (Fig. 1) [7–9]. The high diagnostic accuracy of CEUS in liver imaging is based on two characteristics:

1. the detection and early enhancement of a malignant liver lesion during the arterial phase
2. the rapid wash-out of the contrast agent in malignant liver lesions.

A further benefit of US contrast agents in the clinical routine is their good safety profile, which enables the administration of contrast agents to patients who have contra-indications for contrast-enhanced CT or MRI (e.g. patients with severe renal dysfunction). As a consequence, focal liver diseases have evolved into the single most important

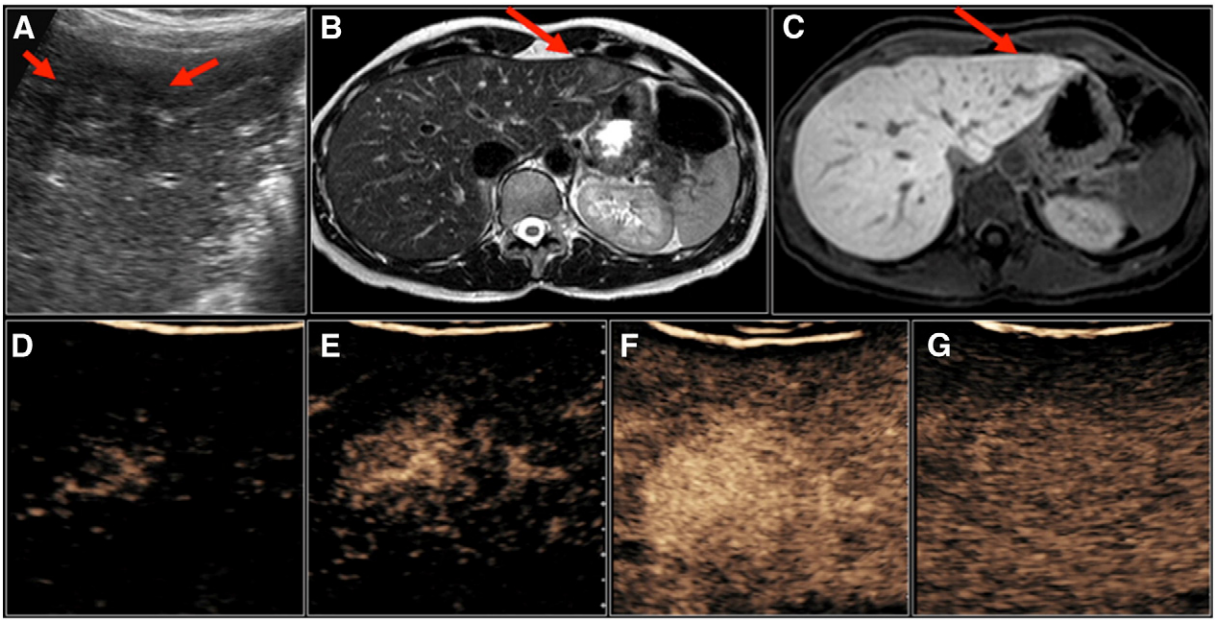

Fig. 1. Examples for the use of CEUS in clinical liver imaging in comparison with MRI. A + B: In B-mode US and in T_2-weighted MRI, a benign liver tumor (fibronodular hyperplasia, FNH) can be delineated. C: Twenty minutes after the administration of the hepatocyte-specific MR contrast agent Gd-EOB-DTPA, the lesion and the surrounding tissue provide comparable contrast enhancement, which is typical for a FNH. D–F: In contrast-specific US mode, one can depict the rapid centrifugal ("spoke-wheel") enhancement of the lesions. In the late phase (G; i.e. 180 s after injection), the lesion provides no wash-out pattern. Knowledge on the microbubble (MB) kinetics in the late phase enables the exclusion a malignant tumor. The enhancement pattern in the arterial phase further supports the diagnosis of a FNH.

application of CEUS. The recommendations for CEUS for liver imaging are summarized in the guidelines for good clinical practice of the EFSUMB [10].

A second major clinical application is contrast echocardiography, where MBs are used for left ventricular opacification and endocardial border delineation. The superior anatomical delineation of the cardiac boarders leads to specific clinical scenarios in which US contrast agents could/should be used, including the assessment of left ventricular systolic function, elevation of the left ventricular apex, mechanical complications of myocardial infarction and the characterization of intracardiac masses. The consensus statement on the use of ultrasound contrast agents was published in 2008 by the American Society of Echocardiography [11] and a summary of the clinical impact of the guidelines was provided two years afterwards [12].

In neurology and intensive care medicine, contrast-enhanced transcranial Doppler ultrasound has been established as a reliable tool to evaluate the cerebral circulation, e.g. to outline vessel stenosis and occlusion as well as ultimately, to diagnose brain death [13,14].

Besides liver, cardiac and brain imaging, indications for CEUS have expanded to applications in the kidney [15,16], in vesico-ureteric reflux [17,18], in the pancreas [18–21], in trauma patients [22] and in cerebral circulation, as well as in oncological studies [23,24]. In this context, an emerging clinical field might represent the assessment of novel targeted drugs such as anti-angiogenic therapies. Here, contrast enhanced ultrasound enables the early identification of responders to an antiangiogenic treatment for gastrointestinal stromal tumors, renal cell carcinoma, and hepatocellular carcinoma [25,26]. Despite this promising data derived in clinical trials, however, a broad application into the daily clinical routine has not yet been established.

In this context, the continuous revision of the existing "Guidelines for Good Clinical Practice" in consensus meetings of the US societies and the continuous medical training of "CEUS-examiners" in specialized CEUS courses are – besides advancements in US machines and contrast agents – the most important preconditions for maintaining and increasing the clinical success of CEUS.

2. Molecular US imaging

An important precondition for in vivo molecular imaging is the use of contrast agents which can be detected with high sensitivity and specificity. MB applied for US imaging fulfill these demands. In principle, even a single MB can be detected and there are imaging techniques that detect MB selectively (see Section 2.2). Due to their size, which typically ranges from 1 to 5 μm, MBs do not extravasate from the vasculature. This is both an advantage and a disadvantage. On the one hand, no unspecific accumulation in the interstitial space is observed, leading to a low unspecific background signal when performing molecular US imaging. On the other hand, since there is no extravasation, only intravascular targets can be addressed, which significantly narrows the diagnostic options. Nevertheless, there are many intravascular targets suitable to characterize angiogenesis and inflammation, which can significantly help to better diagnose diseases and monitor therapy responses. The following sub-sections elaborate on preferentially used targets for molecular US imaging, on the design of MB for molecular imaging purposes and on MB-specific US imaging techniques.

2.1. Targets and contrast agents

2.1.1. Targets

Common targets for molecular US imaging are surface receptor molecules expressed on the luminal side of activated endothelium, either in response to inflammatory or to angiogenic stimuli. Inflammation is accompanied by the recruitment and transmigration of leukocytes through the endothelium to the site of inflammation. This process includes the successive interaction of adhesion molecules on activated endothelial cells with leukocytes. While endothelial- and platelet-specific E- and P-selectins promote the initial attachment and rolling of circulating leukocytes, the adhesion molecules ICAM-1 (intercellular adhesion molecule 1) and VCAM-1 (vascular cell adhesion molecule 1) mediate the firmer adhesion of leukocytes to the endothelium, in order to allow for transmigration. The up-regulation of these adhesion molecules is induced by inflammatory cytokines such as TNF-α (tumor necrosis factor-α) and interleukins (e.g. IL-1). Furthermore, since they are expressed on the luminal side of blood vessels, these adhesion molecules represent prominent targets for molecular US imaging of inflammation-associated processes (as described in Section 2.3 "Applications of CEUS for molecular imaging and drug delivery").

Besides inflammation, also angiogenesis is an important process involving changes in the expression pattern and the behavior of endothelial cells. Angiogenesis is triggered in hypoxic tumor areas via the over-expression of angiogenic factors like vascular endothelial growth factor (VEGF) or fibroblast growth factor (FGF), and it is a crucial prerequisite for tumor growth beyond a size of a few cubic millimeters [27,28]. The most prominent angiogenesis-related targets in molecular US imaging are VEGFR2 receptors and $\alpha_v\beta_3$ integrins. VEGFR2-mediated signaling stimulates endothelial cell proliferation and angiogenesis, and enhances the permeability of blood vessels, thus playing a crucial role in developmental and pathological angiogenesis, e.g. in tumor angiogenesis [29]. VEGF and VEGF-receptors are known to be over-expressed in malignant tumors and their enhanced expression generally correlates with poor clinical outcome [30]. Due to its strong up-regulation during tumor angiogenesis and its almost absence on quiescent endothelial cells, VEGFR2 represents a highly attractive target for molecular US imaging of tumor angiogenesis.

$\alpha_v\beta_3$ integrins belong to the integrin family of heterodimeric surface glycoproteins, mediating cell adhesion to components of the extracellular matrix. In addition to their adhesive functions, integrins are involved in various signaling pathways and thus influence the proliferation and survival of cells, including endothelial cells. Like VEGFR2, the expression of $\alpha_v\beta_3$ integrins is elevated on activated endothelium during angiogenesis, while it is only weakly expressed by quiescent endothelial cells [31,32]. $\alpha_v\beta_3$ integrins recognize different extracellular matrix components (e.g. vitronectin, fibronectin, fibrinogen) via their RGD-binding-site and thus mediate the adhesion of endothelial cells to the extracellular matrix. Blockade of $\alpha_v\beta_3$-mediated cell–matrix interactions between endothelial cells and the extracellular matrix induces apoptosis of endothelial cells [32]. In addition, direct interactions between activated $\alpha_v\beta_3$ integrins and VEGFR2, as well as intracellular signaling cross-talk, have been reported to crucially regulate the VEGF-induced angiogenic response in endothelial cells [33].

Another surface glycoprotein used for molecular US imaging is endoglin, a co-receptor of the transforming growth factor (TGF)-beta receptor. Endoglin is upregulated during inflammation and angiogenesis, and plays an important role in vascular remodeling, homeostasis and angiogenesis [34]. Endoglin expression is considered as a marker for cancer aggressiveness, as a negative correlation was found between the amount of endoglin-expressing blood vessels and the overall survival and metastasis in patients suffering from different types of solid tumors [34].

Apart from the well established inflammation and angiogenesis related markers discussed above, the feasibility of several other targets for CEUS has been tested preclinically. Amongst others, specific approaches include the targeting of prostate specific membrane antigen (PSMA) and thymocyte differentiation antigen-1 for pancreatic cancer imaging [35,36] and glycoprotein IIb/IIIa for imaging of inflammatory thrombosis [37].

2.1.2. US contrast agents

US contrast agents are gas-filled MB with diameters between 1 and 5 μm. Due to their size, MBs have optimal acoustic responses in the MHz range used for US imaging. MBs also possess the capability of

going through small blood capillaries in the body, but stay strictly intravascular. In order to increase the circulation time and reduce the risk side effect that can arise from coalesced gas bubbles, MBs are stabilized by a shell usually made of lipids [38], proteins [39], polymers [40,41] or a mixture of these [42,43]. Apart from the shell, the type of gas in the MB plays an important role in the stability and consequently the circulation time of the constructs. In this context, low solubility gases (such as perfluorochemicals) have been shown to substantially increase the stability and circulation times of MB in vivo [44]. In addition to its stabilizing function, the shell also determines the extent to which the MB can oscillate during insonication [45]. In this regard, one can distinguish between soft- and hard-shelled MBs, with the former being more flexible and thus more suitable for harmonic (non-linear) imaging, while the latter are more suitable for destructive US imaging procedures, such as Power Doppler US.

US molecular imaging requires the use of target-specific MB that can selectively bind to intravascular targets. This is achieved by attaching specific ligands, mostly antibodies or peptides, to the MB surfaces, which enable MB binding to the respective molecular markers. Such ligand-decorated MB can be produced either by incorporating the specific ligands during MB synthesis, or by attaching the ligands to preformed MB. Details on the production of such target-specific MB are beyond the scope of this manuscript, and have been extensively reviewed by us and other groups [46–48].

2.2. Measurement techniques

In general, the echogenicity of MB is strong enough for their detection in fundamental B-mode imaging. For a better differentiation of MB from tissue echoes, i.e. for a high contrast-to-tissue-ratio, non-linear imaging is applied. This technique was originally developed for non-contrast-enhanced tissue US imaging, resulting in a greater lateral resolution and decreased acoustic noise. Thus, images are clearer, with higher contrast and they show more details [49]. In CEUS, the basis for harmonic or non-linear imaging, is the non-linear oscillation of MB at higher wave amplitudes, i.e. with a low to mid-high mechanical index (MI) [49]. Thereby, the waves backscattered by a MB also consist of higher frequency components compared to the center frequency (f_c) and are called harmonics (e.g. $2f_c$, $3f_c$). There are several techniques to detect the harmonic frequency components of MB. Amongst these, Pulse/Phase Inversion (PI), Amplitude Modulation (AM, also: Power Modulation) and Contrast Pulse Sequencing (CPS) are the most common ones. In PI, two pulses are emitted, with the second pulse 180 degree phase-shifted to the first one [50]. For non-linear scatterers like MB, the summation of the response from the two pulses gives a sum signal, whereas for linear scatterers, like tissue, the responses will be zero (or very close to zero, when summed). In AM, as suggested by the name, the amplitude is modulated rather than the phase, resulting in a similar cancelation of the linear responses [51]. This is also valid during CPS imaging, where three pulses are emitted with the first and the third pulse half of the inverse of the second pulse [52]. These techniques rely on the steady oscillation of MB (stable cavitation) and can therefore be classified as non-destructive imaging techniques.

For molecular US imaging, in most cases, the detection is performed in only one slice (2D) and the late-phase enhancement after the clearance of freely circulating MB from the blood, approximately 5–10 min after the i.v. injection of MB, is detected. Sometimes, some freely circulating MB might be left even after 10 min. Thus, a more accurate method to detect bound MB is the destruction–reperfusion technique, which was originally proposed by Wei et al. for the quantification of tissue perfusion [53], and which is nowadays routinely applied for molecular US imaging [54,55]. Here, 5–10 min after i.v. injection, a set of images of the region of interest is recorded, followed by a high MI pulse, which leads to the disintegration of MB. Immediately afterwards, a second set of images is recorded to detect potentially freely circulating MB. Subtraction of the mean signal intensity (SI) of the second set of images from the mean SI of the first set of images produces the SI of the bound MB.

A further destructive technique is based on imaging the destruction events of stationary, target-bound MB, where the disintegration is induced by Doppler pulses [56]. The high amplitude of the Doppler pulse leads to the destruction of MB, causing an emission of a strong broad-band signal. This signal, referred to as stimulated acoustic emission (SAE), is misinterpreted as movement (loss of correlation LOC) and thus registered as a pseudo Doppler shift signal, which can be quantified. There is a linear correlation of the Doppler signal with the concentration of MB [56]. However, above a certain concentration, the signal is saturated and quantification is not possible anymore. Reinhardt et al. developed a method for the quantification of higher MB concentrations, called sensitive particle acoustic quantification (SPAQ) [57]. This is a 3D technique in which the transducer is being moved stepwise in predefined increments of 50–150 μm over the imaged region. In the small, non-overlapping insonified regions only few MB are destroyed and can thus be quantified (Fig. 2A). This technique has already been successfully applied in several studies [55,58–60]. A major advantage of this technique is the quantification of bound MB throughout a complete volume of interest, e.g. a whole tumor, encompassing possible heterogeneities of molecular marker expression within the whole volume of interest (Fig. 2B). Nevertheless, due to the difference in acoustic signals from MB with different sizes, weak acoustic signals from small (<1 μm) MB could be suppressed thereby leading to mistakes in the quantification.

A combination of molecular US imaging with volumetric scanners, for instance a volumetric breast scanner, is thinkable and would provide more operator-independent, accurate and reproducible information as compared to conventional 2D US [55].

Molecular US imaging is constantly improving, for example with the application of acoustic radiation forces (ARF) to increase MB binding. Acoustically manipulating MB was already introduced by Fowlkes et al. in the early 1990s, suggesting it as means for improved image contrast or for localized drug delivery [61]. Zhao et al. later applied ARF and demonstrated a >25-fold increase in the binding of $\alpha_v\beta_3$ integrin targeted MB to human umbilical vein endothelial cells (HUVEC) in vitro [62]. Subsequently, Rychakk and colleagues and later Frinking and colleagues demonstrated enhanced binding of targeted MB in vivo upon ARF application in experimental models of inflammation and cancer. As compared to normal vessels, they reported a 20-fold increase in binding of P-selectin specific MB to an inflamed femoral artery, as well as an enhanced binding of VEGFR2-targeted MB (BR55) in the vasculature of experimental prostate cancers in rats respectively [63,64]. All of the abovementioned methods have been applied in many preclinical studies and show the potential of applying molecular US imaging for improving diagnosis, disease staging and localized image-guided drug delivery (see below; Sections 2.3 and 4.1). Moreover, the first step toward molecular US imaging in clinical settings has already been taken; in a phase 0 clinical trial, BR55 MB has been used to identify regions of VEGFR2 expression in human prostate cancer [65].

2.3. Applications of CEUS for molecular imaging and drug delivery

Molecular US imaging of E-selectin, P-selectin, ICAM-1 or VCAM-1 has been successfully applied for imaging alterations in the endothelium that occur during the process of acute and chronic inflammation. Recently, ischemic myocardium was successfully identified by MB against P- and E-selectins due to their enhanced accumulation [66,67]. In a mouse model of atherosclerosis, VCAM-1-specific MB specifically bound to the inflamed endothelium at the site of the aortic plaque, and MB attachment correlated very well with disease stage [66]. Similarly, Masseau and colleagues showed that CEUS and VCAM-1-taregted MB can also be applied to monitor vascular inflammation in pigs [68]. VCAM-1- as well as P-selectin-specific MBs furthermore showed a high sensitivity for the early detection of the atherogenic

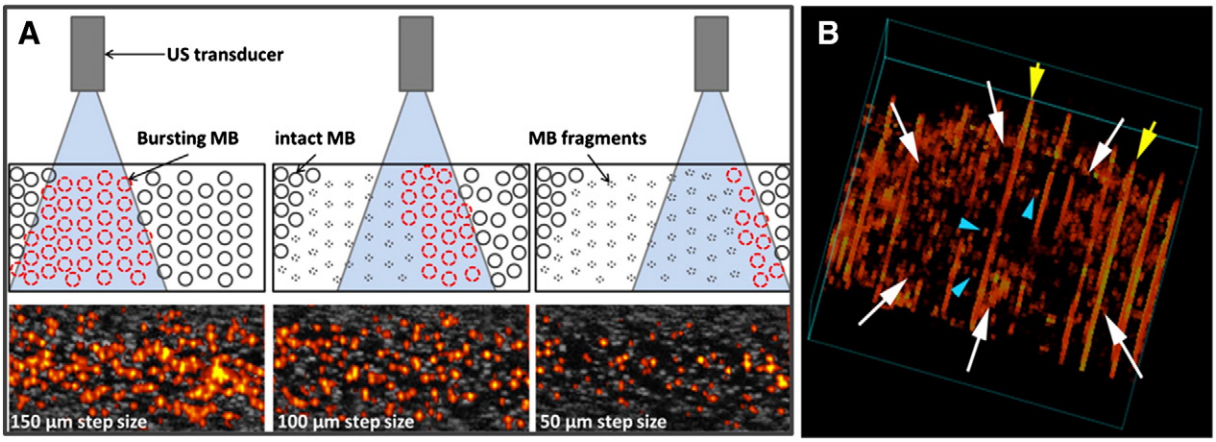

Fig. 2. 3D molecular ultrasound imaging with SPAQ, showing the principle of SPAQ imaging (A). Stepwise movement of the US-transducer leads to MB destruction in the overlapping slice. Smaller step sizes yield less saturated and therefore better quantifiable images. (B) Shows a 3D-reconstructed SPAQ image of VEGFR2-targeted MB binding in an experimental breast cancer xenograft. White arrows outline the tumor. Yellow arrows show artifacts due to breathing of the mouse. The MB-destruction events are displayed as red dots (see e.g. blue arrowheads). The higher VEGFR2 expression at the angiogenic tumor margin compared with the tumor center is clearly demonstrated.

phenotype even before obstructive atherosclerotic lesions appeared [69]. Direct thrombus detection was achieved by MB targeting to glycoprotein IIb/IIIa receptors on clotted platelets [70]. Targeting activated glycoprotein IIb/IIIa using a single-chain antibody on the surface of phospholipid MB also enabled to track the reduction of thrombus size during antithrombotic urokinase therapy in carotid arteries of mice, which were exposed to a ferric chloride injury [71]. Furthermore, novel MB functionalized with a recombinant P-selectin glycoprotein ligand-1 (PSGL-1) analog, which binds to both E- and P-selectins, showed an even stronger binding to the inflamed endothelium after intramuscular injection of endotoxin compared to antibody-coupled or sialyl Lewis X-containing MB [72].

Even more frequently than for imaging inflammation, molecular US imaging is employed for monitoring tumor angiogenesis, including for the assessment of various therapeutic drugs on the vasculature [73–75]. For a broader characterization of angiogenesis, more than one angiogenic marker has been addressed in different studies. Using MB against endoglin, $\alpha_v\beta_3$ integrin and VEGFR2, the varying marker expression during angiogenesis could be longitudinally recorded in breast, ovarian and pancreatic cancer xenografts [76]. MBs against the VEGF/VEGFR-complex, VEGFR2 and endoglin were used for monitoring angiogenesis, as well as the effects of anti-angiogenic treatment or chemotherapy in a mouse model of pancreatic carcinoma. In this context, the binding of the targeted MB significantly decreased upon therapy, correlating with the vascularity of the tumors and with the expression of surface markers [77]. Similarly, a significantly lower accumulation of VEGFR2- and $\alpha_v\beta_3$ integrin-targeted MBs was recorded in human squamous cell carcinoma xenografts upon inhibition of matrix-metalloproteinases [60]. Immunohistochemical analyses revealed that the general decrease in vascularization was responsible for the lower MB binding, rather than the decline in VEGFR2 or $\alpha_v\beta_3$ integrin expression on the endothelium, strongly suggesting the additional analysis of functional parameters such as the relative blood volume when evaluating molecular marker expression by US [60]. Furthermore, simultaneous imaging of two markers using dual-targeted MB against VEGFR2 and $\alpha_v\beta_3$ integrin showed a stronger retention in the tumor endothelium of ovarian cancer xenografts than single-targeted MB [78].

In most of the abovementioned examples of targeting the angiogenesis marker VEGFR2, the ligands were bound to MB via (strept)avidin-biotin coupling. However, since (strept)avidin-biotin coated MBs are not recommended for clinical use due to their potential immunogenicity, MB functionalized by covalently integrated binding epitopes are favored for clinical applications. The first clinically evaluated molecular MB type is BR55, where a heterodimeric peptide against VEGFR2 has been directly integrated in the phospholipid shell. BR55 showed a strong accumulation in the tumor vasculature of breast [79] and prostate cancer xenografts [80], and could sensitively record the decrease in angiogenic activity during therapy using an anti-VEGF antibody in a colon cancer xenograft model [81]. Furthermore, BR55 showed a high sensitivity for discriminating the angiogenic activity of two differentially aggressive breast carcinomas in mice, as well as for assessing the angiogenic activity in evolving breast cancers of very small sizes (Fig. 3) [82]. In addition, molecular US with BR55 was highly sensitive and specific in differentiating benign from malignant breast lesions in a transgenic mouse model of mammary carcinoma, and enabled the detection of ductal carcinomas in situ and invasive breast cancers with high accuracy [83]. An interventional (phase 0) clinical trial has been performed in patients with respect to the potential of BR55 for identifying VEGFR2 positive areas in prostate cancer lesions [65]. There are a number of other US contrast agents that are potentially suited for use in humans. For example, in a more experimental stage, is another lipid (DSPC, palmitic acid and DSPE-PEG_{2000})-coated MB, targeted to E-/P-selectin by thiol bonding of PSGL-1 on the MB surface. These MBs have been used in mice with inflammatory bowel disease, and for quantifying the level of inflammation as well as for monitoring the response to anti-inflammatory treatments [84].Similarly, we recently developed potentially clinically translatable E-selectin-specific poly(n-butyl cyanoacrylate) (PBCA) MBs by covalent (amine) bonding of a short E-selectin-specific peptide with the recognition sequence IELLQAR to the MB surfaces. Significant binding of these MBs was shown in vitro on HUVEC stimulated with TNF-α, as well as in vivo using human ovarian carcinoma bearing mice [85].

Although the abovementioned MB formulations with a direct ligand conjugation provide a valuable platform for clinical translation, the actual clinical implementation of such MB formulations still requires a rigid, time consuming and cost intensive clinical trials process.

3. Multimodal US imaging

3.1. Multimodal US contrast agents

Multimodal US contrast agents are particularly useful in (whole-body) biodistribution and histological validation studies. In this context, they enable the non-invasive and quantitative imaging of the fate of MB and of their shell fragments after systemic application. The ability to image drugs released from MB in vivo and ex vivo, to investigate the coverage of MB surfaces with targeting ligands, to characterize the binding of targeted MB to cells, and to image the opening of biological

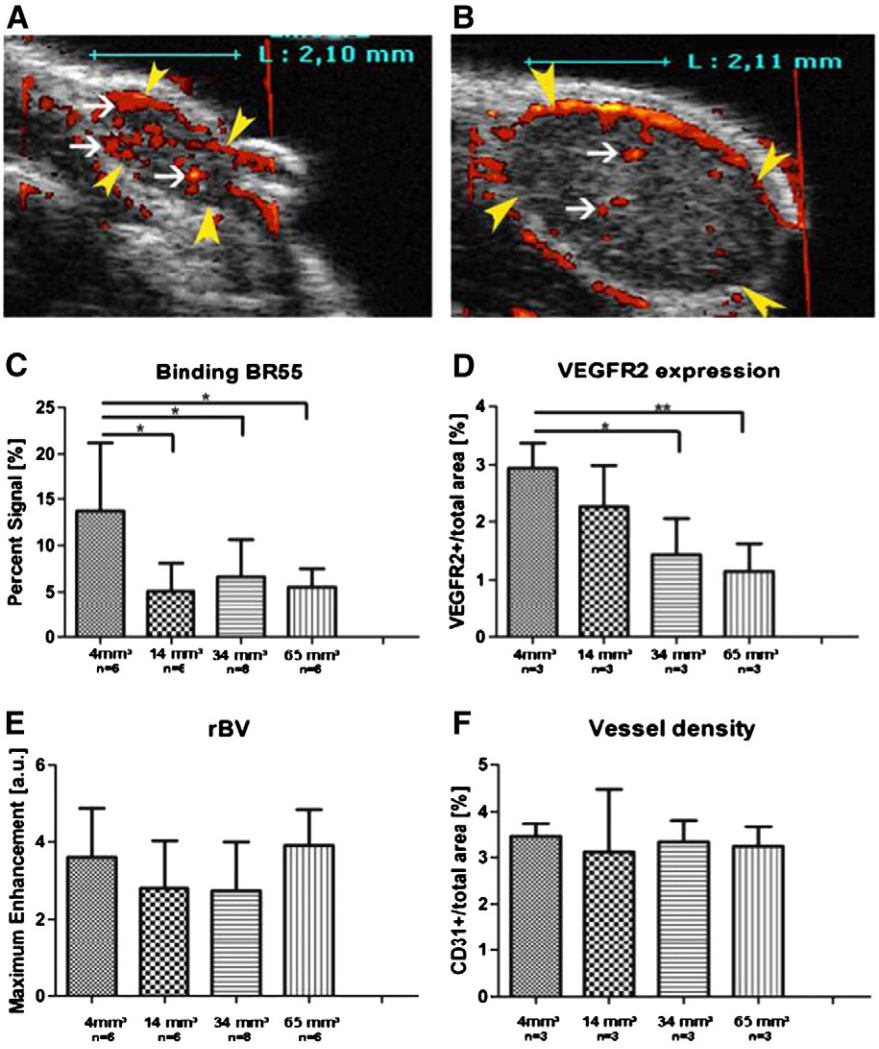

Fig. 3. BR55 highly sensitively depicts very early breast cancer lesions. Representative SPAQ images of one slice in a 4 mm^3 (A) and 34 mm^3 (B) MCF-7 tumor (tumor marked by yellow arrowheads; white arrows show representative signals of destructed BR55 MB (red overlay)). Quantitative analysis of 3D SPAQ imaging demonstrates the highest binding of BR55 in 4 mm^3 small tumors and a significantly reduced binding in larger tumors (C), whereas the relative blood volume (rBV) is constant (E). US data were confirmed by immunohistochemistry (D, F). $^*p < 0.05$; $^{**}p < 0.01$.
Adapted with permission from [82].

barriers (such as cellular membranes and the blood–brain barrier (BBB)) after US-mediated MB destruction are further application fields of multimodal US contrast agents, which will be elaborated upon in this section.

In principle, multimodal US contrast agents make use of the entrapment, attachment or adsorption of other imaging agents (mostly nanoparticles (NP), radiotracers and small molecules, such as fluorescent dyes for optical imaging) in or on the shell of MB. Because the shell presents the only means of combining MB with other imaging agents, the shell properties (thickness, charge etc) are directly related to the amount of agents that can be entrapped. In this context, polymeric shells (~50–500 nm thick) can entrap more imaging agents compared to protein (~15–150 nm thick) and lipid shells (~3 nm thick) [42,86]. So far, the synthesis of multimodal US contrast agents has involved the addition of imaging agents for different modalities during MB synthesis by mechanical agitation [87,88], as well as by the use of microfluidic devices [89,90]. Alternatively, imaging agents can also be coupled by chemical bonding or by passive entrapment on preformed MB [91]. To date, US has been combined with several other imaging modalities, as exemplarily discussed below.

3.2. US–magnetic resonance imaging

Magnetic resonance imaging (MRI) provides whole body images of tissues based on the change in relaxation of the constituent water protons under the influence of an external magnetic field. Apart from its ability to make whole body images, MRI also provides excellent soft-tissue contrast, making a combination of MRI with US highly advantageous. Contrast agents for US and MRI dual-modality imaging feature MB loaded with magnetic species. For example, Liu et al. developed and characterized PBCA-based polymeric MB containing ultrasmall superparamagnetic iron oxide (USPIO) nanoparticles (NP) by a one-pot polymerization reaction, and subsequently showed both in vitro and in vivo that such hybrid MBs are suitable contrast agents for both US and MRI (Fig. 4A–C) [87]. Similarly, USPIO-containing MBs have been synthesized by layer-by-layer deposition as well as by a double emulsion polymerization process [91,92]. Interestingly, UPSIO-containing MBs were observed to have a stronger non-linear response under US treatment compared to standard MB. This phenomenon could be attributed to the increased resistance to compression of NP-loaded MB compared to

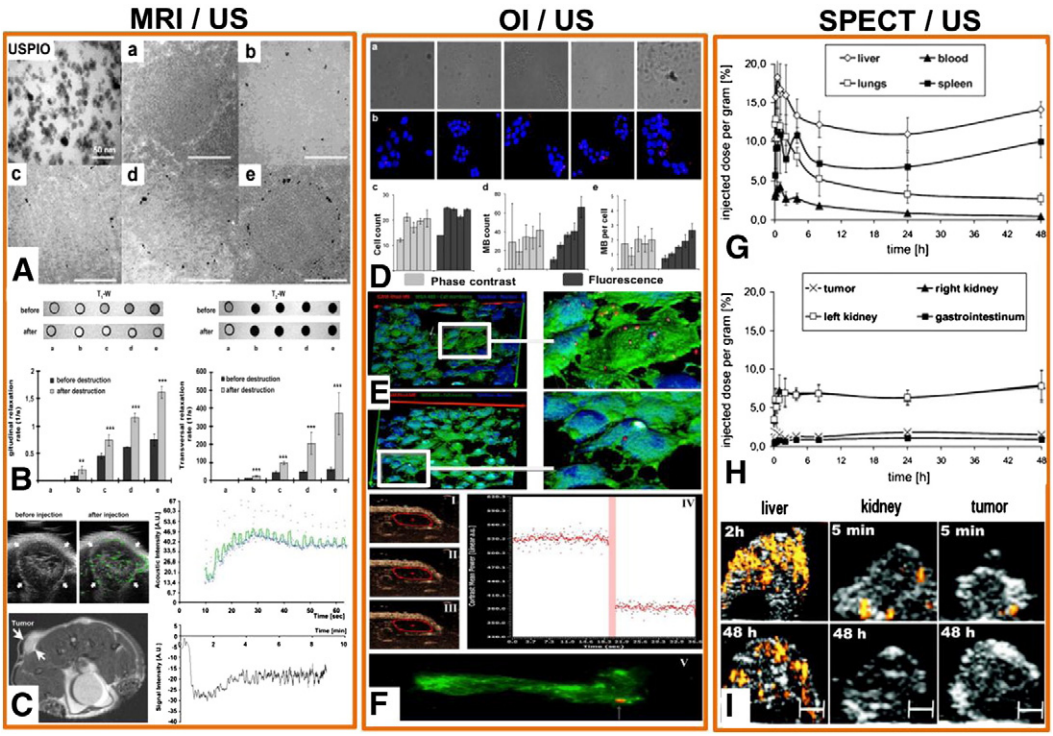

Fig. 4. Multimodal US contrast agents. USPIO-loaded PBCA MB as contrast agents for MRI/US showing TEM images of PBCA MB with increasing USPIO (a–e) concentrations (A), phantom MR imaging showing signal enhancement in MRI, which increases with MB destruction (B), and signal enhancement observed in vivo in both US and MRI upon the i.v. injection of USPIO-loaded MB in tumor bearing mice (C; adapted with permission from [87]). D–F: rhodamine-b loaded PBCA MB for use in optical and US imaging. Comparison between fluorescent and non-fluorescent MB for the evaluation of targeted-MB binding to cells in vitro (D). Two-photon microscopic validation and evaluation of ICAM-1 targeted MB binding to activated (upper panel) vs non-activated (bottom panel) HUVEC (E). Panel F shows the application of fluorescent MB for validation of in vivo molecular US studies. I–III represent sections of the tumor during molecular imaging, while IV shows the evaluation of bound MB by destruction replenishment analysis. By subsequent fluorescence microscopy of tumor cryosections, the attachment of fluorescent MB (red) to FITC-lectin-stained (green) tumor vasculature (V) could be validated (adapted with permission from [101]). Biodistribution analysis of ^{111}In-labeled PBCA-MB over time by gamma counting (G–H) and US (I). Both modalities showed a high amount of MB accumulated in the liver compared to kidney and tumor. Unlike gamma counting, where both signals from MB and shell fragments are registered and quantified over time, upon SPAQ imaging, all MBs are destroyed and cannot be monitored longitudinally by US. Radioactively labeled MBs therefore provide a more reliable means for quantitatively monitoring the biodistribution of MB and their shell fragment in vivo over time as compared to US (adapted with permission from [107]).

their expansion, which leads to non-linear oscillations of the NP-loaded MB [90].

While the studies discussed thus far have made use of the thick shell of polymeric MB for loading NP for MRI, some studies suggested lipid-shelled MB for the same purpose [93,94]. For instance, Fan et al. created US–MRI contrast agents by using superparamagnetic iron oxide (SPIO) NP modified with a four-carbon-atom-long aliphatic terminal end, thus enabling hydrophobic interactions between the SPIO NP and the phospholipids composing the MB shell. They subsequently showed that their constructs provide good contrast enhancement in both US imaging and MR imaging. The deposition of magnetic NP and doxorubicin (encapsulated by electrostatic interaction within the MB shell) in brain tissue after focused US treatment was a further feature of their study, highlighting the ability to open up and deliver drugs across the BBB with such a probe [94].

Another concept for dual-modality MB was proposed by Feshitan et al., who produced Gd^{3+}-DOTA carrying MB by post-modification of pre-formed lipid-shelled MBs [95]. In their study, lipid (90 % DSPE, 10 % DSPE-PEG_{2000}) -shelled MBs were synthesized by sonication, followed by a covalent coupling of DOTA (1,4,7,10-tetraazacyclododecane-1,4,7,10-tetraacetic acid) to the MB shell surface. Subsequently, the complexation of Gd^{3+} ions to the DOTA on the MB surface was performed. A loading of 7.5×10^5 Gd^{3+} ions per μm^2 of the MB surface could be achieved. Interestingly, MR signal enhancement was only observed after MB destruction. The authors attribute this to the limited access of bulk-water to lipid head-groups containing Gd^{3+} for the intact MB compared to the lipid fragments [95,96].

3.3. Photoacoustic (PA)–US imaging

Photoacoustic (PA) imaging is based on the excitation of tissue chromophores using a short-pulsed laser beam, which leads to thermoelastic expansion of the tissue and thus wideband ultrasonic emission. The emitted ultrasonic waves are then captured by an ultrasonic transducer and utilized for image reconstruction. This thereby bestows PA imaging with the molecular sensitivity of optical imaging and the spatial resolution of US imaging [97]. The contrast agents for PA imaging are chromophores such as hemoglobin, indocyanine green (ICG), india ink, and gold nanorods. The combination of PA with US imaging is still in its infancy [98–100], but has already been shown to be useful at the preclinical level for staging deep vein thrombosis [99] and sentinel lymph node mapping [100].

3.4. US–optical imaging

US–OI contrast agents have been prepared by incorporating OI contrast agents (mostly organic dyes and quantum dots) during MB synthesis or into preformed MB, leading to their encapsulation within the MB shell [101,102]. Such dye-loaded fluorescent MBs have been predominantly used for in vitro studies. In this context, US/OI probes are very useful, e.g. to quantify the surface coverage of MB with targeting ligands [41]. US/OI probes can also be used to study MB binding kinetics to biological targets and to investigate the fate of bubbles after intravenous administration. In this regard, Koczera et al. showed that fluorescence analysis instead of phase contrast microscopy can reduce user-

dependency and variability in the quantification of bound target-specific MB to cells in cell culture (Fig. 4D). In addition, they demonstrated that fluorescent MB can be used for in vivo and ex vivo validation. In this context, using two-photon laser scanning microscopy, the binding of rhodamine-loaded, ICAM-1 targeted MB to activated HUVEC was reported (Fig. 4E). Additionally, by fluorescence microscopy, the attachment of targeted rhodamine-loaded MB to tumor endothelium could be validated in histological sections (Fig. 4F) [101]. For theranostic purposes, organic dyes have also been used as model drugs to investigate the loading capacity of such small molecules into the MB shell, as well as their release upon US-mediated MB destruction (see below) [103,104].

A very innovative application of fluorescently labeled MB was presented by Yuan in 2009 [105]. Here, a fluorophore quencher-labeled MB system was used to measure external pressure. The authors claim that pressure variations as low as 1 mm Hg can be measured. If reliably working in vivo, such systems may become interesting tools in oncology research, e.g. to study the impact of pressure on tumor spread and metastasis.

3.5. US–nuclear imaging

Radiolabeled MBs for PET/SPECT–US imaging are generally used for investigating the biodistribution of MB after i.v. injection [106–108]. In comparison to OI, nuclear imaging techniques offer better quantification, which is particularly true in biodistribution analyses. A problem with both OI and nuclear imaging, however, is that intact MBs and their fragments cannot be distinguished. In this context, Palmowski et al. labeled PBCA-MB with ^{111}In by incorporating it into DTPA attached to the MB shell. After i.v. injection, they measured the activity in different organs of mice over several time points up to 48 h post-injection (Fig. 4G–H). While the activity in the liver and spleen stayed relatively high throughout the experiment, the values in lungs and blood decreased over time. In comparison to the liver and spleen, the authors reported much less signal for tumor, gastrointestinal tract and kidney (Fig. 4H). Despite the activity detected in the kidneys, there was no activity in urine, which speaks against kidney clearance of PBCA MBs and of their fragments. This was confirmed by the absence of MB signal during US–SPAQ imaging of the kidney 48 h post-injection (Fig. 4I). The activity measured in the kidney therefore likely resulted from accumulated MB fragments [107].

Alternatively, Tartis et al. performed biodistribution studies with soft-shell MB. In their study, they incorporated the ^{18}F-labeled lipid (^{18}F fluorodipalmitin) to the shell of lipid (DPPC, DPPA, DPPE-PEG$_{5000}$) MB during synthesis. Subsequently, in line with the experiments by Palmowski et al, they demonstrated in male Fischer-344 rats that most of the lipids accumulated in the liver and spleen compared to other organs. Furthermore, they showed that local deposition of ^{18}F-labeled lipids in the kidney is observed upon US-mediated MB destruction [106].

4. Therapeutic and theranostic US

4.1. Therapeutic US

Besides for diagnostic purposes, US can also be used for therapeutic and theranostic purposes. Therapeutic US interventions generally refer to the use of the thermal effects of HIFU. MR-guided HIFU ablation, for instance, is currently used in the clinic for the treatment of deep-seated tumors [5,6,109]. In this procedure, the unwanted tissue is destroyed by heating it to around 60 °C using HIFU. This is nowadays performed under the guidance of MRI which provides high-resolution anatomical images for the delineation of target tissue, as well as real-time temperature mapping, ensuring ablation of only the target region [110,111]. Voogt et al. recently used this technique for ablation of uterine fibroids in 33 patients [109].

Besides for thermal therapy, the effects of US can also be used to trigger release of therapeutic substances from nanocarriers at the target site. In principle, US-induced mild hyperthermia (40–45 °C) is known to increase tissue perfusion, thus e.g. enhancing the deposition of systemically administered therapeutics in the heated tissue. Heating by US can furthermore also be used for target-specific controlled release of therapeutic substances from e.g. temperature-sensitive liposomes [112–114].

Alternatively, also non-thermal effects of US have been used for therapeutic purposes. For example, US-induced MB cavitation has been shown to facilitate thrombolysis. In this regard, representative studies have been performed by Molina et al., who demonstrated in patients with middle cerebral artery (MCA) occlusion that the combination of tissue plasminogen activator (tPA), MB and US treatment was significantly more effective than tPA plus US treatment or tPA alone for thrombolysis [115].

Similarly, therapeutic agents could be released from nanocarriers by non-thermal effects of US. In this context, Wang et al. reported that the hydrolysis of THPMA side chains in PEG-b-THPMA diblock copolymer micelles destabilized the micelles, and enabled the triggered release of Nile red [116]. In line with this, also for PLA-b-PEG micelles, Zhang et al. pointed out that HIFU-induced degradation of the copolymer was responsible for micelle disruption [117]. Recently, Deckers et al. reported radiation force-induced acoustic streaming to be one of the main mechanisms behind the release of hydrophobic and lipophilic substances from liposomes and the release of Nile red from polymeric micelles in vitro [118,119]. In vivo, pulsed HIFU was shown to reversibly enhance the extravasation and the interstitial transport of large (~100 nm) nanospheres in murine muscle [120,121]. Based on their investigations and previous studies, Hancock et al. pointed out acoustic radiation forces as the underlining mechanism behind the enhanced extravasation of nanospheres observed [121].

4.2. Theranostic US

Theranostic refers to the combination of disease diagnosis (in its broadest sence) and therapy [122–124]. Theranostic agents can provide valuable information of drug delivery, drug release and drug efficacy [107]. The ability to perform functional and molecular US, and the possibility to create MB carrying therapeutic substances, therefore makes CEUS an attractive platform for theranostic applications [125,126]. Theranostic US contrast agents are generally synthesized by incorporating therapeutic agents during MB synthesis into the shell of MB [102,127], by the attachment of drug carriers (liposomes, nucleic acid-containing nanoparticles, etc.) to the MB shell surface [128,129] or by partial incorporation of drug containing nano-emulsions into the gas core of the MB [130]. Upon injection, drug-carrying MB can be tracked by US imaging and – upon reaching the target site – destroyed to release their contents using high mechanical index US pulses.

Apart from the ability to track and destroy MB non-invasively by US, the use of MB for theranostics is fueled by the fact that the interaction of US with MB leads to stable (sustained) and inertial (destruction) MB cavitation, which can temporally increase vascular and cellular membrane permeability (sonoporation), thereby potentially increasing the extravasation and/or internalization of co-administered or MB-entrapped drugs. As depicted in Fig. 5, the temporal opening of endothelial and cellular linings can be the result of:

1. Acoustic micro-streaming
2. Stable cavitation; expanding MB pushing the endothelial and/or cellular lining apart
3. Stable cavitation; contracting MB causing invaginations in the lining
4. Inertial cavitation; MB destruction-related shock waves permeabilizing the lining.

The duration for which the permeabilized endothelial and/or cellular membranes remain open is a subject of ongoing research [121,131–133],

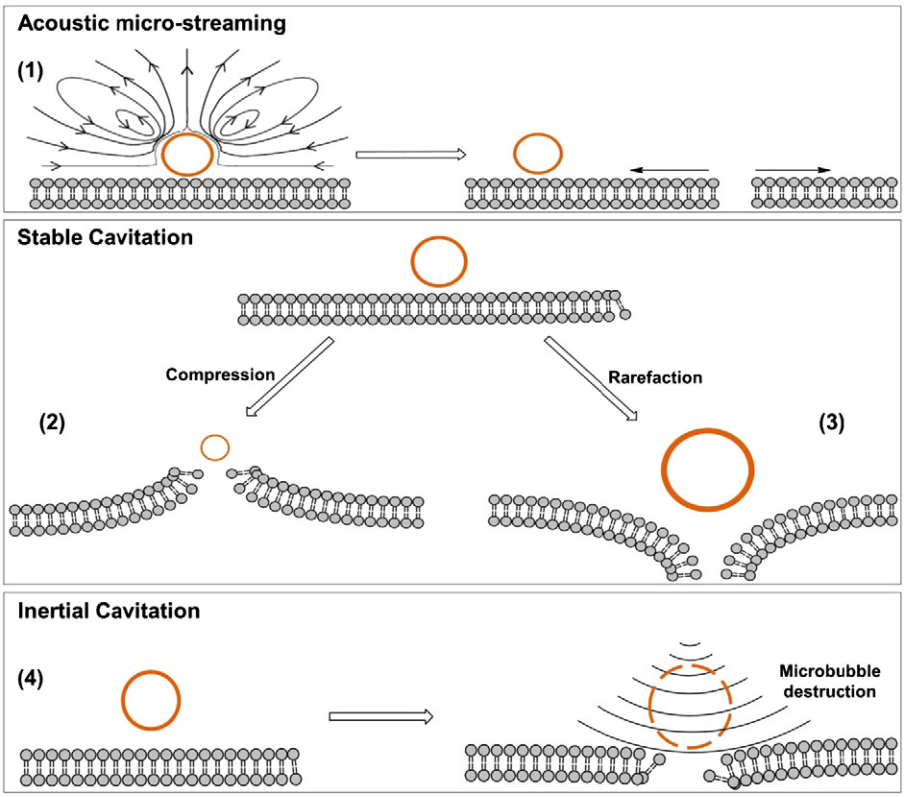

Fig. 5. Mechanisms of sonoporation. Acoustic micro-streaming under stable cavitation (1). (2) MB compression leading to invagination and membrane opening. (3) MB expansion leading to membrane extension (push-force) and opening. (4) MB destruction releasing acoustic shock-waves and jet-streams that permeabilize the membranes.
Adapted with permission from [134].

but extensive pre-clinical studies have made use of this phenomenon to deliver drugs and genes to diseased tissues in oncology, across the BBB, and in thrombolysis.

4.2.1. Drug delivery

Image-guided drug delivery with MB can be performed either by the co-administration of both drugs and MB, or by the injection of drug-loaded MB. The latter has the advantage of reduced systemic drug exposure, and therefore less damage to healthy tissues. A further advantage is in the delivery of nucleic acids, which will otherwise be rapidly degraded upon systemic injection. However, in comparison to the systemic injection of high amounts of therapeutic drugs or their targeted delivery using nanomedicine formulations, the absolute accumulation of drugs delivered to the pathological site using MB likely is relatively low, due to the very short circulation half-life time of MB, to the fact that MB cannot extravasate and to the limited amount of therapeutic agents that can be loaded into the shell of MB. Nevertheless, such a targeting strategy presents a good avenue for the delivery of highly potent compounds, which otherwise cannot be applied due to the risk of extensive damage to healthy tissue.

Drug-loaded MBs are generally produced by incorporating the drugs during MB synthesis (1-step), or by post-loading the drugs into or onto pre-formed MB (2-step) (Fig. 6A). In this context, Wheatley et al. showed that doxorubicin and paclitaxel can be efficiently loaded into PLGA-based MB by both 1- and 2-step syntheses and demonstrated US-mediated release of the loaded drugs after MB destruction in vitro [103,127]. Similarly, Fokong et al. developed PBCA-based MB loaded with hydrophilic (rhodamine-b) and hydrophobic (coumarine-6) model drugs (Fig. 6C–D), and demonstrated efficient US-mediated release of these agents in vitro and in vivo in tumor-bearing mice (Fig. 6E–F) [102]. Alternatively, Kooiman et al. encapsulated a lipophilic model drug (Sudan black) into polymeric MB by using a hexadecane oil (as the drug carrier) in the air core of the bubbles [130]. An additional and very elegant MB design for drug delivery purposes utilized the attachment of drug-carrying liposomes to pre-formed MB (Fig. 6B), which has the advantage of having much higher drug contents per microbubble as compared to the other MB-based materials [128,129]. Yet another theranostic approach to drug delivery using MB was presented by Rapoport and colleagues, who prepared doxorubicin-loaded perfluoropentane-based nanobubbles. Upon injection, these nanobubbles passively accumulated in tumors via EPR, coalesced into MB at physiologic temperatures, and could then be imaged and destroyed by US, releasing encapsulated doxorubicin and resulting in effective tumor growth inhibition [135].

Apart from the use of drug-loaded MB for target-specific delivery to tumors, the advantage of using MB for facilitating site-specific drug delivery and drug therapy has also been utilized for the delivery of therapeutic entities into the CNS. To the end, the combination of MB and destructive US pulses has been reported to enhance drug delivery across the BBB [136–139]. In a recent representative study, Fan et al. demonstrated that using lipid-shelled (DSPC, DSPE-PEG_{2000}, DSPG) MBs loaded with doxorubicin and SPIO in combination with focused US enhanced targeted drug delivery in rats bearing brain gliomas [94]. They observed a significant opening of the BBB in normal brain tissue for animals that received MB and focused US treatment by looking at the extravasation of Evans blue dye (Fig. 6G). Using H&E staining, they confirmed the absence of brain hemorrhage in the tumor and in normal brain tissue (Fig. 6H and J). Furthermore, significant doxorubicin and SPIO deposition was observed for the MB plus focused US treated groups compared to control groups (Fig. 6I and K). While this study provides proof-of-principle for BBB permeabilization and drug delivery into the CNS using focused US and MB, it also might also present a novel avenue for image-guided drug delivery across the BBB by deposited SPIO particles.

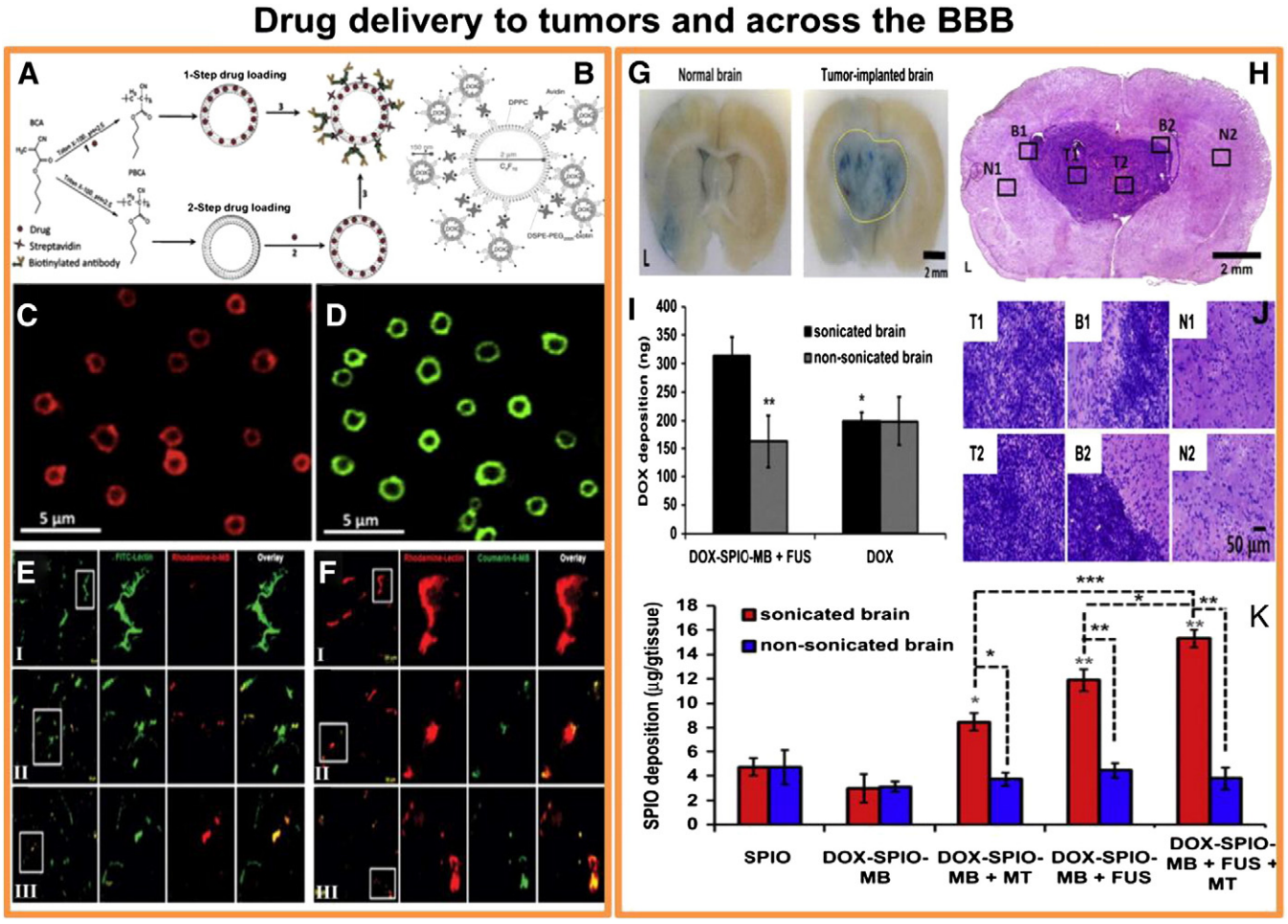

Fig. 6. Drug delivery to tumors and across the BBB using (model)-drug loaded MB. A–B: The entrapment of drug molecules in the MB shell can either be achieved during MB synthesis or upon post-loading. C–D: By fluorescence microscopy, the encapsulation of in the MB shell was validated. E–F: Upon US-mediated destruction of VEGFR2-targeted model drug-loaded MB in tumors, the accumulation of rhodamine-b and coumarine-6 in and around tumor blood vessels for animals treated with MB plus US (panels II and III; vs. without US, panel I) exemplified effective model drug delivery upon US guidance and triggering (adapted with permission from [102]). G: US- plus MB-mediated drug delivery across the BBB was studied using lipid-shelled MB. The extravasation of Evans blue dye was used as verification of BBB-opening induced by DOX–SPIO-MB with US in normal brain tissue and C6 tumors (delineated by yellow line) H–J: H&E stained images of tumor-bearing brain after applying DOX–SPIO-MB and US validated the absence of brain hemorrhage. Region of interest for further analysis was selected from the tumor (T1, T2), the tumor-tissue boundary (B1, B2), and normal brain tissue (N1, N2). Panel I demonstrates increases in doxorubicin accumulation in brain tissue in the DOX–SPIO-MB + US group compared to the DOX group. K: SPIO accumulation in US-treated brain tissues also increased upon the combined application of MB plus US (adapted with permission from [94]).

5. Conclusion

In summary, with the introduction of MB as US contrast agents, important diagnostic and therapeutic options have emerged for this extensively used, real-time and low-cost imaging modality. Besides a detailed characterization of tissue (and tumor) microvascularisation, US imaging also allows the assessment of specific molecular alterations, in particular at the vascular level. This is expected to improve the accuracy in pathology characterization and likely also enables more efficient treatment monitoring. The first molecularly targeted MBs have now entered clinical trials and several others are ready to be tested. Additionally, many promising preclinical studies have demonstrated the capability of MB to increase vascular and cellular permeability, and to thereby facilitate the transport of drugs and genes. Furthermore, several therapeutic US-based interventions, such as MR-guided HIFU, are currently entering the clinic, and a number of theranostic means for image-guided and/or US-triggered drug delivery are currently being evaluated. It therefore seems reasonable to assume that MB, in combinations with diagnostic, therapeutic and theranostic US, will gain ever more importance in the years to come, both at the preclinical level and in patients.

Acknowledgments

This work was financially supported by the DFG (KI 1072/5-1), the ERS Boost Fund (RWTH Aachen), the HighTech.NRW/EU Ziel 2 program (EFRE) ForSaTum, and the ERC (Starting Grant 309495 —NeoNaNo).

References

[1] K.K. Shung, Diagnostic ultrasound: past, present, and future, J. Med. Biol. Eng. 31 (2011) 371–374.
[2] G.M. von Reutern, M.W. Goertler, N.M. Bornstein, M. Del Sette, D.H. Evans, A. Hetzel, M. Kaps, F. Perren, A. Razumovky, M. von Reutern, T. Shiogai, E. Titianova, P. Traubner, N. Venketasubramanian, L.K. Wong, M. Yasaka, Grading carotid stenosis using ultrasonic methods, Stroke 43 (2012) 916–921.
[3] J.A. Baker, M.S. Soo, The evolving role of sonography in evaluating solid breast masses, Semin. Ultrasound CT MR 21 (2000) 286–296.
[4] D.O. Cosgrove, K.E. Chan, Renal transplants: what ultrasound can and cannot do, Ultrasound Q. 24 (2008) 77–87[quiz 141-142].
[5] A.J. Coleman, J.E. Saunders, A review of the physical properties and biological effects of the high amplitude acoustic field used in extracorporeal lithotripsy, Ultrasonics 31 (1993) 75–89.
[6] O. Al-Bataineh, J. Jenne, P. Huber, Clinical and future applications of high intensity focused ultrasound in cancer, Cancer Treat. Rev. 38 (2012) 346–353.
[7] D. Strobel, K. Seitz, W. Blank, A. Schuler, C.F. Dietrich, A. von Herbay, M. Friedrich-Rust, T. Bernatik, Tumor-specific vascularization pattern of liver

metastasis, hepatocellular carcinoma, hemangioma and focal nodular hyperplasia in the differential diagnosis of 1,349 liver lesions in contrast-enhanced ultrasound (CEUS), Ultraschall Med. 30 (2009) 376–382.
[8] K. Seitz, D. Strobel, T. Bernatik, W. Blank, M. Friedrich-Rust, A. Herbay, C.F. Dietrich, H. Strunk, W. Kratzer, A. Schuler, Contrast-enhanced ultrasound (CEUS) for the characterization of focal liver lesions —prospective comparison in clinical practice: CEUS vs. CT (DEGUM multicenter trial). Parts of this manuscript were presented at the Ultrasound Dreilandertreffen 2008, Davos, Ultraschall Med. 30 (2009) 383–389.
[9] K. Seitz, T. Bernatik, D. Strobel, W. Blank, M. Friedrich-Rust, H. Strunk, C. Greis, W. Kratzer, A. Schuler, Contrast-enhanced ultrasound (CEUS) for the characterization of focal liver lesions in clinical practice (DEGUM Multicenter Trial): CEUS vs. MRI—a prospective comparison in 269 patients, Ultraschall Med. 31 (2010) 492–499.
[10] M. Claudon, D. Cosgrove, T. Albrecht, L. Bolondi, M. Bosio, F. Calliada, J.M. Correas, K. Darge, C. Dietrich, M. D'Onofrio, D.H. Evans, C. Filice, L. Greiner, K. Jager, N. Jong, E. Leen, R. Lencioni, D. Lindsell, A. Martegani, S. Meairs, C. Nolsoe, F. Piscaglia, P. Ricci, G. Seidel, B. Skjoldbye, L. Solbiati, L. Thorelius, F. Tranquart, H.P. Weskott, T. Whittingham, Guidelines and good clinical practice recommendations for contrast enhanced ultrasound (CEUS) —update 2008, Ultraschall Med. 29 (2008) 28–44.
[11] S.L. Mulvagh, H. Rakowski, M.A. Vannan, S.S. Abdelmoneim, H. Becher, S.M. Bierig, P.N. Burns, R. Castello, P.D. Coon, M.E. Hagen, J.G. Jollis, T.R. Kimball, D.W. Kitzman, I. Kronzon, A.J. Labovitz, R.M. Lang, J. Mathew, W.S. Moir, S.F. Nagueh, A.S. Pearlman, J.E. Perez, T.R. Porter, J. Rosenbloom, G.M. Strachan, S. Thanigaraj, K. Wei, A. Woo, E.H. Yu, W.A. Zoghbi, American Society of Echocardiography consensus statement on the clinical applications of ultrasonic contrast agents in echocardiography, J. Am. Soc. Echocardiogr. 21 (2008) 1179–1201[quiz 1281].
[12] K. Wei, Contrast echocardiography: what have we learned from the new guidelines? Curr. Cardiol. Rep. 12 (2010) 237–242.
[13] J. Allendoerfer, C. Tanislav, Diagnostic and prognostic value of contrast-enhanced ultrasound in acute stroke, Ultraschall Med. 29 (Suppl. 4) (2008) S210–S214.
[14] S. Welschehold, F. Geisel, C. Beyer, A. Reuland, T. Kerz, Contrast-enhanced transcranial Doppler ultrasonography in the diagnosis of brain death, J. Neurol. Neurosurg. Psychiatry 84 (2013) 939–940.
[15] H. Tamai, Y. Takiguchi, M. Oka, N. Shingaki, S. Enomoto, T. Shiraki, M. Furuta, I. Inoue, M. Iguchi, K. Yanaoka, K. Arii, Y. Shimizu, H. Nakata, T. Shinka, T. Sanke, M. Ichinose, Contrast-enhanced ultrasonography in the diagnosis of solid renal tumors, J. Ultrasound Med. 24 (2005) 1635–1640.
[16] J.M. Correas, M. Claudon, F. Tranquart, A.O. Helenon, The kidney: imaging with microbubble contrast agents, Ultrasound Q. 22 (2006) 53–66.
[17] K. Darge, Voiding urosonography with ultrasound contrast agents for the diagnosis of vesicoureteric reflux in children. I. Procedure, Pediatr. Radiol. 38 (2008) 40–53.
[18] X.L. Li, G.M. Zeng, L. Shi, J. Liang, Q. Cai, Urban ecological land in Changsha City: its quantitative analysis and optimization, Ying Yong Sheng Tai Xue Bao 21 (2010) 415–421.
[19] C.F. Dietrich, B. Braden, M. Hocke, M. Ott, A. Ignee, Improved characterisation of solitary solid pancreatic tumours using contrast enhanced transabdominal ultrasound, J. Cancer Res. Clin. Oncol. 134 (2008) 635–643.
[20] M. D'Onofrio, A.J. Megibow, N. Faccioli, R. Malago, P. Capelli, M. Falconi, R.P. Mucelli, Comparison of contrast-enhanced sonography and MRI in displaying anatomic features of cystic pancreatic masses, AJR Am. J. Roentgenol. 189 (2007) 1435–1442.
[21] T. Ripolles, M.J. Martinez, E. Lopez, I. Castello, F. Delgado, Contrast-enhanced ultrasound in the staging of acute pancreatitis, Eur. Radiol. 20 (2010) 2518–2523.
[22] O. Catalano, L. Aiani, L. Barozzi, D. Bokor, A. De Marchi, C. Faletti, F. Maggioni, N. Montanari, P.E. Orlandi, A. Siani, P.S. Sidhu, P.K. Thompson, M. Valentino, A. Ziosi, A. Martegani, CEUS in abdominal trauma: multi-center study, Abdom. Imaging 34 (2009) 225–234.
[23] P.G. Sorelli, D.O. Cosgrove, W.E. Svensson, N. Zaman, K. Satchithananda, N.K. Barrett, A.K. Lim, Can contrast-enhanced sonography distinguish benign from malignant breast masses? J. Clin. Ultrasound 38 (2010) 177–181.
[24] C. Balleyguier, P. Opolon, M.C. Mathieu, A. Athanasiou, J.R. Garbay, S. Delaloge, C. Dromain, New potential and applications of contrast-enhanced ultrasound of the breast: own investigations and review of the literature, Eur. J. Radiol. 69 (2009) 14–23.
[25] N. Lassau, L. Chami, M. Chebil, B. Benatsou, S. Bidault, E. Girard, G. Abboud, A. Roche, Dynamic contrast-enhanced ultrasonography (DCE-US) and anti-angiogenic treatments, Discov. Med. 11 (2011) 18–24.
[26] F. Knieling, M.J. Waldner, R.S. Goertz, S. Zopf, D. Wildner, M.F. Neurath, T. Bernatik, D. Strobel, Early response to anti-tumoral treatment in hepatocellular carcinoma—can quantitative contrast-enhanced ultrasound predict outcome? Ultraschall Med. 34 (2013) 38–46.
[27] J. Folkman, Angiogenesis in cancer, vascular, rheumatoid and other disease, Nat. Med. 1 (1995) 27–31.
[28] G. Bergers, L.E. Benjamin, Tumorigenesis and the angiogenic switch, Nat. Rev. Cancer 3 (2003) 401–410.
[29] N. Ferrara, VEGF and the quest for tumour angiogenesis factors, Nat. Rev. Cancer 2 (2002) 795–803.
[30] N. Ferrara, Vascular endothelial growth factor: basic science and clinical progress, Endocr. Rev. 25 (2004) 581–611.
[31] P.C. Brooks, R.A. Clark, D.A. Cheresh, Requirement of vascular integrin alpha v beta 3 for angiogenesis, Science 264 (1994) 569–571.
[32] J.D. Hood, D.A. Cheresh, Role of integrins in cell invasion and migration, Nat. Rev. Cancer 2 (2002) 91–100.
[33] P.R. Somanath, N.L. Malinin, T.V. Byzova, Cooperation between integrin alphavbeta3 and VEGFR2 in angiogenesis, Angiogenesis 12 (2009) 177–185.
[34] J.M. Lopez-Novoa, C. Bernabeu, The physiological role of endoglin in the cardiovascular system, Am. J. Physiol. Heart Circ. Physiol. 299 (2010) H959–H974.
[35] K. Foygel, H. Wang, S. Machtaler, A.M. Lutz, R. Chen, M. Pysz, A.W. Lowe, L. Tian, T. Carrigan, T.A. Brentnall, J.K. Willmann, Detection of pancreatic ductal adenocarcinoma in mice by ultrasound imaging of thymocyte differentiation antigen 1, Gastroenterology 145 (2013) 885–894.
[36] L. Wang, L. Li, Y. Guo, H. Tong, X. Fan, J. Ding, H. Huang, Construction and in vitro/in vivo targeting of PSMA-targeted nanoscale microbubbles in prostate cancer, Prostate 73 (2013) 1147–1158.
[37] W. Wu, Y. Wang, S. Shen, J. Wu, S. Guo, L. Su, F. Hou, Z. Wang, Y. Liao, J. Bin, In vivo ultrasound molecular imaging of inflammatory thrombosis in arteries with cyclic Arg-Gly-Asp-modified microbubbles targeted to glycoprotein IIb/IIIa, Invest. Radiol. 48 (2013) 803–812.
[38] D. Bokor, J.B. Chambers, P.J. Rees, T.G. Mant, F. Luzzani, A. Spinazzi, Clinical safety of SonoVue, a new contrast agent for ultrasound imaging, in healthy volunteers and in patients with chronic obstructive pulmonary disease, Invest. Radiol. 36 (2001) 104–109.
[39] G. Korpanty, P.A. Grayburn, R.V. Shohet, R.A. Brekken, Targeting vascular endothelium with avidin microbubbles, Ultrasound Med. Biol. 31 (2005) 1279–1283.
[40] W. Cui, J. Bei, S. Wang, G. Zhi, Y. Zhao, X. Zhou, H. Zhang, Y. Xu, Preparation and evaluation of poly(L-lactide-co-glycolide) (PLGA) microbubbles as a contrast agent for myocardial contrast echocardiography, J. Biomed. Mater. Res. B Appl. Biomater. 73 (2005) 171–178.
[41] S. Fokong, M. Siepmann, Z. Liu, G. Schmitz, F. Kiessling, J. Gatjens, Advanced characterization and refinement of poly N-butyl cyanoacrylate microbubbles for ultrasound imaging, Ultrasound Med. Biol. 37 (2011) 1622–1634.
[42] S. Sirsi, M. Borden, Microbubble compositions, properties and biomedical applications, Bubble Sci. Eng. Technol. 1 (2009) 3–17.
[43] M.A. Borden, C.F. Caskey, E. Little, R.J. Gillies, K.W. Ferrara, DNA and polylysine adsorption and multilayer construction onto cationic lipid-coated microbubbles, Langmuir 23 (2007) 9401–9408.
[44] E.G. Schutt, D.H. Klein, R.M. Mattrey, J.G. Riess, Injectable microbubbles as contrast agents for diagnostic ultrasound imaging: the key role of perfluorochemicals, Angew. Chem. Int. Ed. Engl. 42 (2003) 3218–3235.
[45] M. Postema, G. Schmitz, Ultrasonic bubbles in medicine: influence of the shell, Ultrason. Sonochem. 14 (2007) 438–444.
[46] F. Kiessling, J. Bzyl, S. Fokong, M. Siepmann, G. Schmitz, M. Palmowski, Targeted ultrasound imaging of cancer: an emerging technology on its way to clinics, Curr. Pharm. Des. 18 (2012) 2184–2199.
[47] S. Unnikrishnan, A.L. Klibanov, Microbubbles as ultrasound contrast agents for molecular imaging: preparation and application, AJR Am. J. Roentgenol. 199 (2012) 292–299.
[48] A.L. Klibanov, Microbubble contrast agents: targeted ultrasound imaging and ultrasound-assisted drug-delivery applications, Invest. Radiol. 41 (2006) 354–362.
[49] C. Kollmann, New sonographic techniques for harmonic imaging—underlying physical principles, Eur. J. Radiol. 64 (2007) 164–172.
[50] D.H. Simpson, C.T. Chin, P.N. Burns, Pulse inversion Doppler: a new method for detecting nonlinear echoes from microbubble contrast agents, IEEE Trans. Ultrason. Ferroelectr. Freq. Control 46 (1999) 372–382.
[51] R.J. Eckersley, C.T. Chin, P.N. Burns, Optimising phase and amplitude modulation schemes for imaging microbubble contrast agents at low acoustic power, Ultrasound Med. Biol. 31 (2005) 213–219.
[52] P.J. Phillips, Contrast pulse sequences (CPS): imaging nonlinear microbubbles, Ultrasonics (2001) 1739–1745.
[53] K. Wei, A.R. Jayaweera, S. Firoozan, A. Linka, D.M. Skyba, S. Kaul, Quantification of myocardial blood flow with ultrasound-induced destruction of microbubbles administered as a constant venous infusion, Circulation 97 (1998) 473–483.
[54] J.K. Willmann, R. Paulmurugan, K. Chen, O. Gheysens, M. Rodriguez-Porcel, A.M. Lutz, I.Y. Chen, X. Chen, S.S. Gambhir, US imaging of tumor angiogenesis with microbubbles targeted to vascular endothelial growth factor receptor type 2 in mice, Radiology 246 (2008) 508–518.
[55] J. Bzyl, M. Palmowski, A. Rix, S. Arns, J.M. Hyvelin, S. Pochon, J. Ehling, S. Schrading, F. Kiessling, W. Lederle, The high angiogenic activity in very early breast cancer enables reliable imaging with VEGFR2-targeted microbubbles (BR55), Eur. Radiol. 23 (2013) 468–475.
[56] K. Tiemann, C. Pohl, T. Schlosser, J. Goenechea, M. Bruce, C. Veltmann, S. Kuntz, M. Bangard, H. Becher, Stimulated acoustic emission: pseudo-Doppler shifts seen during the destruction of nonmoving microbubbles, Ultrasound Med. Biol. 26 (2000) 1161–1167.
[57] M. Reinhardt, P. Hauff, A. Briel, V. Uhlendorf, R.A. Linker, M. Maurer, M. Schirner, Sensitive particle acoustic quantification (SPAQ): a new ultrasound-based approach for the quantification of ultrasound contrast media in high concentrations, Invest. Radiol. 40 (2005) 2–7.
[58] M. Reinhardt, P. Hauff, R.A. Linker, A. Briel, R. Gold, P. Rieckmann, G. Becker, K.V. Toyka, M. Maurer, M. Schirner, Ultrasound derived imaging and quantification of cell adhesion molecules in experimental autoimmune encephalomyelitis (EAE) by Sensitive Particle Acoustic Quantification (SPAQ), Neuroimage 27 (2005) 267–278.
[59] M. Palmowski, P. Peschke, J. Huppert, P. Hauff, M. Reinhardt, M. Maurer, C.P. Karger, M. Scholz, W. Semmler, P.E. Huber, F.M. Kiessling, Molecular ultrasound imaging of early vascular response in prostate tumors irradiated with carbon ions, Neoplasia 11 (2009) 856–863.
[60] M. Palmowski, J. Huppert, G. Ladewig, P. Hauff, M. Reinhardt, M.M. Mueller, E.C. Woenne, J.W. Jenne, M. Maurer, G.W. Kauffmann, W. Semmler, F. Kiessling, Molecular profiling of angiogenesis with targeted ultrasound imaging: early assessment of antiangiogenic therapy effects, Mol. Cancer Ther. 7 (2008) 101–109.

[61] J. Fowlkes, E. Gardner, J. Ivey, P. Carson, The role of acoustic radiation force in contrast enhancement techniques using bubble-based ultrasound contrast agents, J. Acoust. Soc. Am. 93 (1993) 2348.
[62] S. Zhao, M. Borden, S.H. Bloch, D. Kruse, K.W. Ferrara, P.A. Dayton, Radiation-force assisted targeting facilitates ultrasonic molecular imaging, Mol. Imaging 3 (2004) 135–148.
[63] J.J. Rychak, A.L. Klibanov, K.F. Ley, J.A. Hossack, Enhanced targeting of ultrasound contrast agents using acoustic radiation force, Ultrasound Med. Biol. 33 (2007) 1132–1139.
[64] P.J. Frinking, I. Tardy, M. Theraulaz, M. Arditi, J. Powers, S. Pochon, F. Tranquart, Effects of acoustic radiation force on the binding efficiency of BR55, a VEGFR2-specific ultrasound contrast agent, Ultrasound Med. Biol. 38 (2012) 1460–1469.
[65] H. Wijkstra, M. Smeenge, J.J. Rosette, S. de la Pochon, F. Tranquart, Targeted microbubble prostate cancer imaging with BR55, Proceedings of the 17th European Symposium on Ultrasound Imaging, 2012.
[66] B.A. Kaufmann, J.M. Sanders, C. Davis, A. Xie, P. Aldred, I.J. Sarembock, J.R. Lindner, Molecular imaging of inflammation in atherosclerosis with targeted ultrasound detection of vascular cell adhesion molecule-1, Circulation 116 (2007) 276–284.
[67] F.S. Villanueva, E. Lu, S. Bowry, S. Kilic, E. Tom, J. Wang, J. Gretton, J.J. Pacella, W.R. Wagner, Myocardial ischemic memory imaging with molecular echocardiography, Circulation 115 (2007) 345–352.
[68] I. Masseau, M.J. Davis, D.K. Bowles, Carotid inflammation is unaltered by exercise in hypercholesterolemic Swine, Med. Sci. Sports Exerc. 44 (2012) 2277–2289.
[69] B.A. Kaufmann, C.L. Carr, J.T. Belcik, A. Xie, Q. Yue, S. Chadderdon, E.S. Caplan, J. Khangura, S. Bullens, S. Bunting, J.R. Lindner, Molecular imaging of the initial inflammatory response in atherosclerosis: implications for early detection of disease, Arterioscler. Thromb. Vasc. Biol. 30 (2010) 54–59.
[70] P.A. Schumann, J.P. Christiansen, R.M. Quigley, T.P. McCreery, R.H. Sweitzer, E.C. Unger, J.R. Lindner, T.O. Matsunaga, Targeted-microbubble binding selectively to GPIIb IIIa receptors of platelet thrombi, Invest. Radiol. 37 (2002) 587–593.
[71] X. Wang, C.E. Hagemeyer, J.D. Hohmann, E. Leitner, P.C. Armstrong, F. Jia, M. Olschewski, A. Needles, K. Peter, I. Ahrens, Novel single-chain antibody-targeted microbubbles for molecular ultrasound imaging of thrombosis: validation of a unique noninvasive method for rapid and sensitive detection of thrombi and monitoring of success or failure of thrombolysis in mice, Circulation 125 (2012) 3117–3126.
[72] T. Bettinger, P. Bussat, I. Tardy, S. Pochon, J.M. Hyvelin, P. Emmel, S. Henrioud, N. Biolluz, J.K. Willmann, M. Schneider, F. Tranquart, Ultrasound molecular imaging contrast agent binding to both E- and P-selectin in different species, Invest. Radiol. 47 (2012) 516–523.
[73] F. Kiessling, J. Huppert, M. Palmowski, Functional and molecular ultrasound imaging: concepts and contrast agents, Curr. Med. Chem. 16 (2009) 627–642.
[74] N. Deshpande, M.A. Pysz, J.K. Willmann, Molecular ultrasound assessment of tumor angiogenesis, Angiogenesis 13 (2010) 175–188.
[75] A.G. Sorace, R. Saini, M. Mahoney, K. Hoyt, Molecular ultrasound imaging using a targeted contrast agent for assessing early tumor response to antiangiogenic therapy, J Ultrasound Med. 31 (2012) 1543–1550.
[76] N. Deshpande, Y. Ren, K. Foygel, J. Rosenberg, J.K. Willmann, Tumor angiogenic marker expression levels during tumor growth: longitudinal assessment with molecularly targeted microbubbles and US imaging, Radiology 258 (2011) 804–811.
[77] G. Korpanty, J.G. Carbon, P.A. Grayburn, J.B. Fleming, R.A. Brekken, Monitoring response to anticancer therapy by targeting microbubbles to tumor vasculature, Clin. Cancer Res. 13 (2007) 323–330.
[78] J.K. Willmann, A.M. Lutz, R. Paulmurugan, M.R. Patel, P. Chu, J. Rosenberg, S.S. Gambhir, Dual-targeted contrast agent for US assessment of tumor angiogenesis in vivo, Radiology 248 (2008) 936–944.
[79] S. Pochon, I. Tardy, P. Bussat, T. Bettinger, J. Brochot, M. von Wronski, L. Passantino, M. Schneider, BR55: a lipopeptide-based VEGFR2-targeted ultrasound contrast agent for molecular imaging of angiogenesis, Invest. Radiol. 45 (2010) 89–95.
[80] I. Tardy, S. Pochon, M. Theraulaz, P. Emmel, L. Passantino, F. Tranquart, M. Schneider, Ultrasound molecular imaging of VEGFR2 in a rat prostate tumor model using BR55, Invest. Radiol. 45 (2010) 573–578.
[81] M.A. Pysz, K. Foygel, J. Rosenberg, S.S. Gambhir, M. Schneider, J.K. Willmann, Antiangiogenic cancer therapy: monitoring with molecular US and a clinically translatable contrast agent (BR55), Radiology 256 (2010) 519–527.
[82] J. Bzyl, M. Palmowski, A. Rix, S. Arns, J.M. Hyvelin, S. Pochon, J. Ehling, S. Schrading, F. Kiessling, W. Lederle, The high angiogenic activity in very early breast cancer enables reliable imaging with VEGFR2-targeted microbubbles (BR55), Eur. Radiol. 23 (2013) 468–475.
[83] S.V. Bachawal, K.C. Jensen, A.M. Lutz, S.S. Gambhir, F. Tranquart, L. Tian, J.K. Willmann, Earlier detection of breast cancer with ultrasound molecular imaging in a transgenic mouse model, Cancer Res. 73 (2013) 1689–1698.
[84] N. Deshpande, A.M. Lutz, Y. Ren, K. Foygel, L. Tian, M. Schneider, R. Pai, P.J. Pasricha, J.K. Willmann, Quantification and monitoring of inflammation in murine inflammatory bowel disease with targeted contrast-enhanced US, Radiology 262 (2012) 172–180.
[85] S. Fokong, A. Fragoso, A. Rix, A. Curaj, Z. Wu, W. Lederle, O. Iranzo, J. Gatjens, F. Kiessling, M. Palmowski, Ultrasound molecular imaging of E-selectin in tumor vessels using poly n-butyl cyanoacrylate microbubbles covalently coupled to a short targeting peptide, Invest. Radiol. 48 (2013) 843–850.
[86] F. Cavalieri, M. Zhou, M. Tortora, B. Lucilla, M. Ashokkumar, Methods of preparation of multifunctional microbubbles and their in vitro/in vivo assessment of stability, functional and structural properties, Curr. Pharm. Des. 18 (2012) 2135–2151.
[87] Z. Liu, T. Lammers, J. Ehling, S. Fokong, J. Bornemann, F. Kiessling, J. Gatjens, Iron oxide nanoparticle-containing microbubble composites as contrast agents for MR and ultrasound dual-modality imaging, Biomaterials 32 (2011) 6155–6163.
[88] E. Huynh, J.F. Lovell, B.L. Helfield, M. Jeon, C. Kim, D.E. Goertz, B.C. Wilson, G. Zheng, Porphyrin shell microbubbles with intrinsic ultrasound and photoacoustic properties, J. Am. Chem. Soc. 134 (2012) 16464–16467.
[89] M. Seo, I. Gorelikov, R. Williams, N. Matsuura, Microfluidic assembly of monodisperse, nanoparticle-incorporated perfluorocarbon microbubbles for medical imaging and therapy, Langmuir 26 (2010) 13855–13860.
[90] J.I. Park, D. Jagadeesan, R. Williams, W. Oakden, S. Chung, G.J. Stanisz, E. Kumacheva, Microbubbles loaded with nanoparticles: a route to multiple imaging modalities, ACS Nano 4 (2010) 6579–6586.
[91] A.A. Barrefelt, T.B. Brismar, G. Egri, P. Aspelin, A. Olsson, L. Oddo, S. Margheritelli, K. Caidahl, G. Paradossi, L. Dahne, R. Axelsson, M. Hassan, Multimodality imaging using SPECT/CT and MRI and ligand functionalized 99mTc-labeled magnetic microbubbles, EJNMMI Res. 3 (2013) 12.
[92] F. Yang, Y. Li, Z. Chen, Y. Zhang, J. Wu, N. Gu, Superparamagnetic iron oxide nanoparticle-embedded encapsulated microbubbles as dual contrast agents of magnetic resonance and ultrasound imaging, Biomaterials 30 (2009) 3882–3890.
[93] D. Vlaskou, C. Plank, O. Mykhaylyk, Magnetic and acoustically active microbubbles loaded with nucleic acids for gene delivery, Methods Mol. Biol. 948 (2013) 205–241.
[94] C.H. Fan, C.Y. Ting, H.J. Lin, C.H. Wang, H.L. Liu, T.C. Yen, C.K. Yeh, SPIO-conjugated, doxorubicin-loaded microbubbles for concurrent MRI and focused-ultrasound enhanced brain-tumor drug delivery, Biomaterials 34 (2013) 3706–3715.
[95] J.A. Feshitan, F. Vlachos, S.R. Sirsi, E.E. Konofagou, M.A. Borden, Theranostic Gd(III)-lipid microbubbles for MRI-guided focused ultrasound surgery, Biomaterials 33 (2012) 247–255.
[96] J.A. Feshitan, M.A. Boss, M.A. Borden, Magnetic resonance properties of Gd(III)-bound lipid-coated microbubbles and their cavitation fragments, Langmuir 28 (2012) 15336–15343.
[97] L.V. Wang, Prospects of photoacoustic tomography, Med. Phys. 35 (2008) 5758–5767.
[98] R.X. Xu, Multifunctional microbubbles and nanobubbles for photoacoustic imaging, Contrast Media Mol. Imaging 6 (2011) 401–411.
[99] A.B. Karpiouk, S.R. Aglyamov, S. Mallidi, J. Shah, W.G. Scott, J.M. Rubin, S.Y. Emelianov, Combined ultrasound and photoacoustic imaging to detect and stage deep vein thrombosis: phantom and ex vivo studies, J. Biomed. Opt. 13 (2008) 054061.
[100] T.N. Erpelding, C. Kim, M. Pramanik, L. Jankovic, K. Maslov, Z. Guo, J.A. Margenthaler, M.D. Pashley, L.V. Wang, Sentinel lymph nodes in the rat: noninvasive photoacoustic and US imaging with a clinical US system, Radiology 256 (2010) 102–110.
[101] P. Koczera, Z. Wu, S. Fokong, B. Theek, L. Appold, S. Jorge, D. Möckel, Z. Liu, A. Curaj, G. Storm, M. Zandvoort, F. Kiessling, T. Lammers, Fluorescently labeled microbubbles for facilitating translational molecular ultrasound studies, Drug Delivery and, Transl. Res. 2 (2012) 56–64.
[102] S. Fokong, B. Theek, Z. Wu, P. Koczera, L. Appold, S. Jorge, U. Resch-Genger, M. van Zandvoort, G. Storm, F. Kiessling, T. Lammers, Image-guided, targeted and triggered drug delivery to tumors using polymer-based microbubbles, J. Control. Release 163 (2012) 75–81.
[103] J.R. Eisenbrey, O.M. Burstein, R. Kambhampati, F. Forsberg, J.B. Liu, M.A. Wheatley, Development and optimization of a doxorubicin loaded poly(lactic acid) contrast agent for ultrasound directed drug delivery, J. Control. Release 143 (2010) 38–44.
[104] R. Deckers, A. Yudina, L.C. Cardoit, C.T. Moonen, A fluorescent chromophore TOTO-3 as a 'smart probe' for the assessment of ultrasound-mediated local drug delivery in vivo, Contrast Media Mol. Imaging 6 (2011) 267–274.
[105] B. Yuan, Sensitivity of fluorophore-quencher labeled microbubbles to externally applied static pressure, Med. Phys. 36 (2009) 3455–3469.
[106] M.S. Tartis, D.E. Kruse, H. Zheng, H. Zhang, A. Kheirolomoom, J. Marik, K.W. Ferrara, Dynamic microPET imaging of ultrasound contrast agents and lipid delivery, J. Control. Release 131 (2008) 160–166.
[107] M. Palmowski, B. Morgenstern, P. Hauff, M. Reinhardt, J. Huppert, M. Maurer, E.C. Woenne, S. Doerk, G. Ladewig, J.W. Jenne, S. Delorme, L. Grenacher, P. Hallscheidt, G.W. Kauffmann, W. Semmler, F. Kiessling, Pharmacodynamics of streptavidin-coated cyanoacrylate microbubbles designed for molecular ultrasound imaging, Invest. Radiol. 43 (2008) 162–169.
[108] N. Lazarova, P.W. Causey, J.A. Lemon, S.K. Czorny, J.R. Forbes, A. Zlitni, A. Genady, F.S. Foster, J.F. Valliant, The synthesis, magnetic purification and evaluation of 99mTc-labeled microbubbles, Nucl. Med. Biol. 38 (2011) 1111–1118.
[109] M.J. Voogt, H. Trillaud, Y.S. Kim, W.P. Mali, J. Barkhausen, L.W. Bartels, R. Deckers, N. Frulio, H. Rhim, H.K. Lim, T. Eckey, H.J. Nieminen, C. Mougenot, B. Keserci, J. Soini, T. Vaara, M.O. Kohler, S. Sokka, M.A. van den Bosch, Volumetric feedback ablation of uterine fibroids using magnetic resonance-guided high intensity focused ultrasound therapy, Eur. Radiol. 22 (2012) 411–417.
[110] B. Quesson, J.A. de Zwart, C.T. Moonen, Magnetic resonance temperature imaging for guidance of thermotherapy, J. Magn. Reson. Imaging 12 (2000) 525–533.
[111] H.E. Cline, K. Hynynen, C.J. Hardy, R.D. Watkins, J.F. Schenck, F.A. Jolesz, MR temperature mapping of focused ultrasound surgery, Magn. Reson. Med. 31 (1994) 628–636.
[112] G.A. Koning, A.M. Eggermont, L.H. Lindner, T.L. ten Hagen, Hyperthermia and thermosensitive liposomes for improved delivery of chemotherapeutic drugs to solid tumors, Pharm. Res. 27 (2010) 1750–1754.
[113] H. Grull, S. Langereis, Hyperthermia-triggered drug delivery from temperature-sensitive liposomes using MRI-guided high intensity focused ultrasound, J. Control. Release 161 (2012) 317–327.
[114] N.M. Hijnen, E. Heijman, M.O. Kohler, M. Ylihautala, G.J. Ehnholm, A.W. Simonetti, H. Grull, Tumour hyperthermia and ablation in rats using a clinical MR-HIFU

system equipped with a dedicated small animal set-up, Int. J. Hyperthermia 28 (2012) 141–155.
[115] C.A. Molina, M. Ribo, M. Rubiera, J. Montaner, E. Santamarina, R. Delgado-Mederos, J.F. Arenillas, R. Huertas, F. Purroy, P. Delgado, J. Alvarez-Sabin, Microbubble administration accelerates clot lysis during continuous 2-MHz ultrasound monitoring in stroke patients treated with intravenous tissue plasminogen activator, Stroke 37 (2006) 425–429.
[116] J. Wang, M. Pelletier, H. Zhang, H. Xia, Y. Zhao, High-frequency ultrasound-responsive block copolymer micelle, Langmuir 25 (2009) 13201–13205.
[117] H. Zhang, H. Xia, J. Wang, Y. Li, High intensity focused ultrasound-responsive release behavior of PLA-b-PEG copolymer micelles, J. Control. Release 139 (2009) 31–39.
[118] C. Oerlemans, R. Deckers, G. Storm, W.E. Hennink, J.F. Nijsen, Evidence for a new mechanism behind HIFU-triggered release from liposomes, J. Control. Release 168 (2013) 327–333.
[119] R. Deckers, A. Paradissis, C. Oerlemans, M. Talelli, G. Storm, W.E. Hennink, J.F. Nijsen, New insights into the HIFU-triggered release from polymeric micelles, Langmuir 29 (2013) 9483–9490.
[120] B.E. O'Neill, H. Vo, M. Angstadt, K.P. Li, T. Quinn, V. Frenkel, Pulsed high intensity focused ultrasound mediated nanoparticle delivery: mechanisms and efficacy in murine muscle, Ultrasound Med. Biol. 35 (2009) 416–424.
[121] H.A. Hancock, L.H. Smith, J. Cuesta, A.K. Durrani, M. Angstadt, M.L. Palmeri, E. Kimmel, V. Frenkel, Investigations into pulsed high-intensity focused ultrasound-enhanced delivery: preliminary evidence for a novel mechanism, Ultrasound Med. Biol. 35 (2009) 1722–1736.
[122] T. Lammers, S. Aime, W.E. Hennink, G. Storm, F. Kiessling, Theranostic nanomedicine, Acc. Chem. Res. 44 (2011) 1029–1038.
[123] T. Lammers, F. Kiessling, W.E. Hennink, G. Storm, Nanotheranostics and image-guided drug delivery: current concepts and future directions, Mol. Pharm. 7 (2010) 1899–1912.
[124] K.H. Martin, P.A. Dayton, Current status and prospects for microbubbles in ultrasound theranostics, Wiley Interdiscip. Rev. Nanomed. Nanobiotechnol. 5 (2013) 329–345.
[125] S.R. Sirsi, M.A. Borden, Advances in ultrasound mediated gene therapy using microbubble contrast agents, Theranostics 2 (2012) 1208–1222.
[126] F. Kiessling, S. Fokong, P. Koczera, W. Lederle, T. Lammers, Ultrasound microbubbles for molecular diagnosis, therapy, and theranostics, J. Nucl. Med. 53 (2012) 345–348.
[127] M.C. Cochran, J. Eisenbrey, R.O. Ouma, M. Soulen, M.A. Wheatley, Doxorubicin and paclitaxel loaded microbubbles for ultrasound triggered drug delivery, Int. J. Pharm. 414 (2011) 161–170.
[128] I. Lentacker, B. Geers, J. Demeester, S.C. De Smedt, N.N. Sanders, Design and evaluation of doxorubicin-containing microbubbles for ultrasound-triggered doxorubicin delivery: cytotoxicity and mechanisms involved, Mol. Ther. 18 (2010) 101–108.
[129] A.L. Klibanov, T.I. Shevchenko, B.I. Raju, R. Seip, C.T. Chin, Ultrasound-triggered release of materials entrapped in microbubble-liposome constructs: a tool for targeted drug delivery, J. Control. Release 148 (2010) 13–17.
[130] K. Kooiman, M.R. Bohmer, M. Emmer, H.J. Vos, C. Chlon, W.T. Shi, C.S. Hall, S.H. de Winter, K. Schroen, M. Versluis, N. de Jong, A. van Wamel, Oil-filled polymer microcapsules for ultrasound-mediated delivery of lipophilic drugs, J. Control. Release 133 (2009) 109–118.
[131] A. van Wamel, K. Kooiman, M. Harteveld, M. Emmer, F.J. ten Cate, M. Versluis, N. de Jong, Vibrating microbubbles poking individual cells: drug transfer into cells via sonoporation, J. Control. Release 112 (2006) 149–155.
[132] R.K. Schlicher, H. Radhakrishna, T.P. Tolentino, R.P. Apkarian, V. Zarnitsyn, M.R. Prausnitz, Mechanism of intracellular delivery by acoustic cavitation, Ultrasound Med. Biol. 32 (2006) 915–924.
[133] A. Yudina, M. Lepetit-Coiffe, C.T. Moonen, Evaluation of the temporal window for drug delivery following ultrasound-mediated membrane permeability enhancement, Mol. Imaging Biol. 13 (2011) 239–249.
[134] S.P. Wrenn, S.M. Dicker, E.F. Small, N.R. Dan, M. Mleczko, G. Schmitz, P.A. Lewin, Bursting bubbles and bilayers, Theranostics 2 (2012) 1140–1159.
[135] N. Rapoport, Z. Gao, A. Kennedy, Multifunctional nanoparticles for combining ultrasonic tumor imaging and targeted chemotherapy, J. Natl. Cancer Inst. 99 (2007) 1095–1106.
[136] J. Park, Y. Zhang, N. Vykhodtseva, F.A. Jolesz, N.J. McDannold, The kinetics of blood–brain barrier permeability and targeted doxorubicin delivery into brain induced by focused ultrasound, J. Control. Release 162 (2012) 134–142.
[137] B. Marty, B. Larrat, M. Van Landeghem, C. Robic, P. Robert, M. Port, D. Le Bihan, M. Pernot, M. Tanter, F. Lethimonnier, S. Meriaux, Dynamic study of blood–brain barrier closure after its disruption using ultrasound: a quantitative analysis, J. Cereb. Blood Flow Metab. 32 (2012) 1948–1958.
[138] K. Hynynen, Ultrasound for drug and gene delivery to the brain, Adv. Drug Deliv. Rev. 60 (2008) 1209–1217.
[139] J.J. Choi, K. Selert, F. Vlachos, A. Wong, E.E. Konofagou, Noninvasive and localized neuronal delivery using short ultrasonic pulses and microbubbles, Proc. Natl. Acad. Sci. U. S. A. 108 (2011) 16539–16544.